

Longitudinal molecular imaging of progesterone receptor reveals early differential response to endocrine therapy in breast cancer with an activating *ESR1* mutation

Manoj Kumar¹, Kelley Salem¹, Justin J. Jeffery², Yongjun Yan¹, Aparna M. Mahajan³, Amy M. Fowler^{1,2,4}

¹Department of Radiology, University of Wisconsin School of Medicine and Public Health, 600 Highland Avenue, Madison, WI 53792.

²University of Wisconsin Carbone Cancer Center, 600 Highland Avenue, Madison, WI 53792.

³Department of Pathology and Laboratory Medicine, University of Wisconsin School of Medicine and Public Health, 1685 Highland Avenue, Madison, WI 53705.

⁴Department of Medical Physics, University of Wisconsin School of Medicine and Public Health, 1111 Highland Avenue, Madison, WI 53705.

First Author Information: Manoj Kumar, MS, PhD Candidate, University of Wisconsin-Madison, 600 Highland Avenue, Madison, WI 53792-3252. Phone: 608-262-0118; Email: mkumar9@wisc.edu

Corresponding Author Information: Amy M. Fowler, MD, PhD, Assistant Professor, University of Wisconsin School of Medicine and Public Health, 600 Highland Avenue, Madison, WI 53792-3252. Phone: 608-262-9186; (Fax): 608-265-1836; Email: afowler@uwhealth.org

Financial Support: Clinical and Translational Science Award program, through the NIH National Center for Advancing Translational Sciences, grant UL1TR002373, UW Institute of Clinical and Translational Research KL2 Scholar Award (KL2TR000428), American Cancer Society Institutional Research Grant Pilot Award (IRG-15-213-51), Mary Kay Innovative/Translational Cancer Research Grant

Word count: 4998

Running Title: *ESR1* Mutation Breast Cancer PET Imaging

ABSTRACT

Activating mutations in the estrogen receptor (ER) alpha gene (*ESR1*) result in constitutive transcriptional activity in the absence of estrogen and is associated with endocrine resistance in metastatic ER+ breast cancer. It is not known how activating *ESR1* mutations may alter the predictive values of molecular imaging agents for endocrine therapy response. This study investigated the effect of an activating *ESR1* mutation on pre-treatment ¹⁸F-fluoroestradiol (¹⁸F-FES) uptake and early assessment of endocrine therapy response using ¹⁸F-FDG and ¹⁸F-fluorofuranylnorprogesterone (¹⁸F-FFNP) PET/CT imaging of tumor glucose metabolism and progesterone receptor (PR) expression, respectively.

Methods: ER+PR+ T47D breast cancer cells expressing wild-type (WT)-ER or an activating *ESR1* mutation, Y537S-ER, were used to generate tumor xenografts in ovariectomized female immunodeficient mice supplemented with 17 β -estradiol. Tumor growth curves were determined in the presence or absence of estrogen and for ethanol vehicle control or fulvestrant treatment, a selective ER degrader. Pre-treatment ¹⁸F-FES uptake was compared between Y537S-ER and WT-ER tumors. Longitudinal PET/CT imaging with ¹⁸F-FFNP and ¹⁸F-FDG was performed before and 7 to 9 days after starting endocrine therapy with fulvestrant. Radiopharmaceutical uptake in Y537S-ER and WT-ER tumors were compared between baseline and follow-up scans. Statistical significance was determined using paired t-tests for longitudinal imaging and two-way ANOVA for ¹⁸F-FFNP tissue biodistribution assay.

Results: Y537S-ER xenografts showed estrogen-independent growth, while WT-ER tumors grew only with estrogen. Fulvestrant treatment for 28 days significantly reduced tumor volumes for WT-ER, but only stabilized volumes for Y537S-ER. Baseline ¹⁸F-FES uptake was not significantly different between WT-ER and Y537S-ER tumors. Fulvestrant treatment induced a

similar early metabolic response for both WT-ER and Y537S-ER tumors. ^{18}F -FFNP uptake in WT-ER tumors was significantly reduced after 7 days of fulvestrant treatment; however, this reduction did not occur in Y537S-ER tumors which showed no significant change between baseline and follow-up PET/CT.

Conclusion: Molecular imaging of PR expression dynamics could be a non-invasive approach for early identification of reduced effectiveness of endocrine therapy resulting from activating *ESR1* mutations.

Key Words:

- *ESR1* mutation
- Fulvestrant
- ^{18}F -FFNP PET/CT
- ^{18}F -FDG
- ^{18}F -FES

INTRODUCTION

Estrogen receptor alpha (ER) and progesterone receptor (PR) are expressed in the majority of breast cancer and are prognostic and predictive biomarkers. Immunohistochemical assessment of these biomarkers is performed clinically as indication for endocrine therapy. Patients with metastatic ER+ or PR+ breast cancer can be treated with various endocrine therapy agents such as aromatase inhibitors or selective ER modulators like tamoxifen. Selective ER degraders is another option which are pure ER antagonists, competitively inhibiting ER binding with estrogen and targeting ER protein for proteasome-mediated degradation. Fulvestrant is the only FDA-approved drug in this class for the treatment of ER+ metastatic breast cancer. While most patients with metastatic ER+ breast cancer have a favorable response to endocrine therapy initially, the response rate decreases with subsequent lines of therapy indicating the development of resistance (1).

Up to 40% of patients with metastatic ER+ breast cancer treated with endocrine therapy have acquired somatic mutations in the ER alpha gene (*ESR1*) which correlate with reduced survival (2,3). Most *ESR1* mutations occur at amino acids 537 and 538 in the ligand-binding domain (4). These mutations mimic an agonist-bound receptor conformation resulting in constitutive transcriptional activity in the absence of estrogen (5,6). Of the reported mutations, Tyrosine-537-Serine (Y537S) has high prevalence, has maximal estrogen-independent transcriptional activity, and is more resistant to ER antagonists (7,8). The conformational change in the ligand-binding domain also impacts ligand binding affinity with reduced binding of Y537S-ER to estradiol and fulvestrant compared to wild-type ER (4,7). Higher doses of fulvestrant are required to inhibit Y537S-ER transcriptional activity and cell proliferation compared to wild-type ER (7-11). Emergence of *ESR1* tumor mutations driving endocrine

resistance is a significant problem as there are currently no clinically-approved therapies that target *ESR1* mutations.

Clinical studies of imaging biomarkers to predict response to endocrine therapy have primarily focused on ER using ^{18}F -fluoroestradiol (^{18}F -FES) and glucose metabolism using ^{18}F -fluorodeoxyglucose (^{18}F -FDG) (12-18). Preclinical studies have also identified ^{18}F -fluorofuranylnorprogesterone, ^{18}F -FFNP, a radiolabeled progestin analog that binds to progesterone receptor (PR), as a potential biomarker of estrogen sensitivity and endocrine therapy response (19-21). PR is a downstream target of activated ER and an indicator of ER functionality such that when ER transcriptional function is blocked, PR protein expression decreases. A study investigating ^{18}F -FFNP PET imaging in breast cancer has demonstrated its safety, dosimetry, and correlation between uptake and tumor PR status, thus supporting its translational potential (22).

It is not known how activating *ESR1* mutations in ER+ metastatic breast cancer may alter the predictive values of molecular imaging agents for endocrine therapy response. In this study, we investigated how expression of Y537S-ER impacts the predictive values of ^{18}F -FES, ^{18}F -FDG, and ^{18}F -FFNP. Given the constitutive transcriptional activity and reduced endocrine sensitivity of the mutant receptor, we hypothesized that suppression of ^{18}F -FFNP uptake and inhibition of tumor glycolytic activity will be impaired in tumors expressing Y537S-ER treated with fulvestrant.

MATERIALS AND METHODS

Cell Culture

Experiments adhered to a protocol approved by the Office of Biological Safety. CRISPR-Cas9 genome-edited T47D cells with wild-type and *ESR1* knock-in of Y537S were kindly provided by Dr. Steffi Oesterreich (University of Pittsburgh) (10) and tested negative for murine pathogens and Mycoplasma (IDEXX BioResearch). Cells were cultured in Roswell Park Memorial Institute medium (Corning) with 10% fetal bovine serum (VWR) and 1% penicillin/streptomycin (Gibco) at 37 °C and 5% CO₂. Steroid hormone-depleted conditions consisted of 10% charcoal/dextran stripped fetal bovine serum in phenol red-free media with 1% penicillin/streptomycin and 2% L-glutamine.

Droplet Digital PCR

Reactions (Supplemental Material) were performed using QX200 Droplet Digital PCR System (Bio-Rad). Mutation allele fractions were determined using QuantaSoft Analysis Pro v1.0.596 (Bio-Rad).

Mice, Tumor Xenografts, and Treatments

Animal studies adhered to American Association for Laboratory Animal Science guidelines following an approved protocol by the Institutional Animal Care and Use Committee. Seven- to 10-week-old female immunodeficient athymic nude mice (NCr-nu/nu, Charles River) were used for all experiments except for the ¹⁸F-FES tissue biodistribution assay, which were NOD *scid* gamma (NSG; UW-Madison, Biotron Laboratory Breeding Core). Cells (3,000,000) were injected into the second thoracic mammary fat pads at 1:1 ratio with Matrigel (BD Biosciences) in 100 μL. Tumor size was measured using calipers and volume was calculated [length * width²]/2].

To assess estrogen-dependent tumor growth, ovariectomized mice were housed with 10 µg/mL 17β-estradiol (E2) in the drinking water or with regular drinking water (19). For fulvestrant treatment studies, ovariectomized mice were subcutaneously implanted with silastic tubing (Dow Corning, 5/64" ID, 1/8" OD, 1.6 cm length) containing 20 µg E2 (60-day release) to support tumor growth. Mice with palpable tumors (>3 mm diameter) were randomized to control and treatment groups. After randomization, no significant difference in tumor volumes between treatment groups was confirmed for each experiment. Mice received subcutaneous twice weekly injections of fulvestrant (4 mg/mouse; Sandoz) or vehicle control (100 µL sunflower oil with ethanol).

Radiopharmaceuticals, Tissue Biodistribution, and Imaging

¹⁸F-FES and ¹⁸F-FFNP were synthesized by the University of Wisconsin-Madison Radiopharmaceutical Production Facility (23). ¹⁸F-FDG was obtained commercially (SOFIE). Molar activity of ¹⁸F-FFNP ranged from 86 to 475 GBq/µmol and ¹⁸F-FES was 200 GBq/µmol at the end of synthesis. ¹⁸F-FES and ¹⁸F-FFNP tissue biodistribution assays were performed 1 hour after tail vein injection. Injected doses (mean ± SD) of ¹⁸F-FES and ¹⁸F-FFNP were 1.14 ± 0.04 MBq (~30 µCi) and 3.17 ± 0.17 MBq (~85 µCi), respectively. Activity in tissues were measured using a gamma counter and data were background-corrected to calculate the percent injected dose per gram (%ID/g). Tumor-to-muscle ratio was calculated as the ratio of the %ID/g of tumor to that of averaged left and right quadriceps muscles.

¹⁸F-FFNP PET/CT was performed at baseline and after 7 days of fulvestrant treatment. To administer equimolar amounts of ¹⁸F-FFNP, mice were injected via tail vein with an average of 3.87 ± 0.12 MBq (~104 µCi) for baseline imaging and 8.70 ± 0.35 MBq (~235 µCi) for

follow-up imaging. For ^{18}F -FDG PET/CT, fasted mice were injected via tail vein with 5.77 ± 0.20 MBq (~ 156 μCi) at baseline and after 9 days of fulvestrant. Mice were anesthetized with 2% isoflurane and scanned supine in the microPET/CT scanner (Inveon, Siemens Preclinical Solutions) 1 hour after injection. Mice for ^{18}F -FDG PET/CT remained anesthetized during the 1-hour uptake time. Scanning and reconstruction parameters were reported previously (24). Volumes of interest were drawn around the tumors, pituitary gland as an internal positive control for estrogen-regulated PR expression (25), and within quadriceps muscles as non-target tissue uptake. Quantitative uptake was expressed as maximum %ID/g.

Histology

Excised tumors were fixed in 10% formalin, embedded in paraffin, and sectioned for staining. Slides were deparaffinized followed by heat epitope retrieval in citrate buffer (pH 6.0) for 60 min at 95 °C. Immunostaining was performed for PR (1:100 NCL-L-PGR-312; Leica Biosystems) and ER (1:100 SP1; Thermo Fisher) using VECTASTAIN ABC HRP Kit (Vector Laboratories). An experienced breast pathologist (A.M.) blinded to the treatment groups evaluated the percentage of tumor cells with positive staining and intensity (none, weak, moderate, strong).

Statistical Analysis

For the longitudinal PET/CT studies, paired t-tests were used to assess change in radiotracer uptake between the two imaging time points for the same tumor within the same mouse. Paired t-tests were used to compare ^{18}F -FES uptake between tumor types within the same mouse. Two-way ANOVA with Tukey post-test was used to analyze the transcriptional activity

results and for the ^{18}F -FFNP tissue biodistribution assay (GraphPad Prism 8). Results are presented as mean \pm standard error. $P < 0.05$ was considered significant.

RESULTS

***In Vitro* Analysis of CRISPR-edited T47D Y537S-ER and WT-ER cells**

The Y537S mutation allele fraction was 50% in Y537S-ER cells, indicating heterozygous knock-in of the mutation, and 0% in WT-ER cells. A 32.7 ± 10.2 -fold increase in transcriptional activity was observed in Y537S-ER cells compared to WT-ER in the absence of estrogen ($p = 0.0195$; Supplemental Fig. 1). Constitutive transcriptional activity observed with Y537S-ER is consistent with published studies (8,10,24).

Effect of Estrogen and Endocrine Therapy on WT-ER and Y537S-ER Tumor Growth

While WT-ER tumor xenografts demonstrated sustained growth only with estrogen, Y537S-ER tumors grew with or without estrogen (Fig. 1A). Furthermore, Y537S-ER tumors without estrogen grew faster than WT-ER tumors with estrogen. Consistent with *in vitro* transcriptional function, the *in vivo* growth of Y537S-ER tumor xenografts is also estrogen independent. The Y537S allele fraction was $52 \pm 2.5\%$ and $0.2 \pm 0.2\%$ in Y537S-ER and WT-ER tumors, respectively, indicating that the heterozygous presence of the mutation is maintained when these cells are grown as tumor xenografts.

Given previous work demonstrating reduced binding affinity of Y537S-ER for fulvestrant with higher doses required to inhibit transcriptional activity and proliferation (7-11), we hypothesized that tumors expressing Y537S-ER would be less sensitive to growth inhibition by fulvestrant compared to WT-ER. A significant reduction in WT-ER tumor volume was observed

by day 10 for fulvestrant-treated mice compared to control ($p=0.003$) (Fig. 1B) with approximately 46% total reduction in volume from baseline to the 28-day endpoint. Y537S-ER tumors in the control group continued to increase over time with approximately 122% total increase in volume. Y537S-ER tumor growth was arrested with fulvestrant treatment, but tumor volumes did not decrease, as was observed for WT-ER tumors. A significant difference in Y537S-ER tumor volumes between treatment groups was observed by day 16 ($p=0.004$). Thus, tumor growth responses with fulvestrant treatment differed between WT-ER (reduced tumor volumes) and Y537S-ER xenografts (stable tumor volumes) indicating that Y537S-ER tumors are less sensitive to growth inhibition by fulvestrant compared to WT-ER.

Predictive Value of Baseline ^{18}F -FES uptake for Therapy Response

Several studies have demonstrated ^{18}F -FES PET imaging as a potential predictive biomarker for endocrine therapy response in patients with metastatic ER+ breast cancer (13,18,26). Thus, we examined whether differences in baseline ^{18}F -FES uptake exist that could predict the differential growth response to fulvestrant between tumor types. There was no significant difference in ^{18}F -FES uptake in Y537S-ER and WT-ER tumors (Fig. 2A). The tumor-to-muscle ratio was 4.56 ± 0.33 for Y537S-ER tumors and 4.21 ± 0.44 for WT-ER tumors ($p=0.2772$) (Fig. 2B). Uterus uptake was 7.89 ± 1.01 %ID/g. Thus, comparable baseline ^{18}F -FES uptake values in Y537S-ER and WT-ER tumors does not provide insight into their different growth responses to fulvestrant treatment.

Longitudinal ^{18}F -FDG PET/CT Assessment of Therapy Response

Metabolic response determined by ^{18}F -FDG PET/CT has been shown in small clinical studies as a potential biomarker of endocrine therapy response (12,15,16,27). Thus, we investigated whether differences in metabolic response exist between Y537S-ER and WT-ER tumors that correspond with the differential growth response to fulvestrant treatment. ^{18}F -FDG PET/CT of mice bearing WT-ER and Y537S-ER xenografts was performed before and after 9 days of fulvestrant treatment, a time point before statistically significant changes in tumor size. Between the baseline and follow-up scans, ^{18}F -FDG uptake decreased for both tumor types (Fig. 3; Supplemental Table 1). Reduction in post-treatment ^{18}F -FDG uptake was $-31.85 \pm 8.18\%$ for WT-ER tumors and $-28.29 \pm 7.69\%$ for Y537S-ER tumors ($p=0.7735$). These data indicate that fulvestrant treatment induces a similar metabolic response in WT-ER and Y537S-ER tumors despite ultimately distinct growth responses.

Longitudinal ^{18}F -FFNP PET/CT Assessment of Therapy Response

We hypothesized that greater suppression of ^{18}F -FFNP uptake would occur in tumors expressing WT-ER compared to Y537S-ER in response to fulvestrant due to reduced binding affinity of Y537S-ER for fulvestrant and reduced treatment efficacy for inhibiting Y537S-ER transcriptional activity previously reported (7-11). ^{18}F -FFNP PET/CT of mice bearing WT-ER and Y537S-ER tumor xenografts was performed before and after 7 days of fulvestrant treatment (Fig. 4; Supplemental Table 2). For WT-ER tumors, ^{18}F -FFNP uptake decreased from 3.97 ± 0.35 at baseline to 2.10 ± 0.20 %ID/g ($p=0.0001$) on the follow-up scan. However, there was no significant change in ^{18}F -FFNP uptake for Y537S-ER tumors between the baseline (4.18 ± 0.37 %ID/g) and follow-up scan 3.92 ± 0.5 %ID/g ($p=0.3326$). Reduction in post-treatment ^{18}F -FFNP

uptake was $-47.86 \pm 2.60\%$ for WT-ER tumors and $-7.04 \pm 8.07\%$ for Y537S-ER tumors ($p=0.0033$). As a positive control for fulvestrant inhibition of ER-regulated PR expression, ^{18}F -FFNP uptake in the pituitary was reduced to 2.07 ± 0.04 %ID/g during treatment compared to 3.05 ± 0.08 %ID/g at baseline ($p=0.0003$) (Supplemental Fig. 2).

To independently confirm these results, a separate cohort of mice bearing Y537S-ER or WT-ER tumor xenografts were used for a tissue biodistribution assay in which ^{18}F -FFNP uptake is directly measured in excised tumors. For WT-ER tumor-bearing mice treated with fulvestrant for 7 days, ^{18}F -FFNP uptake was less than the vehicle control group (1.10 ± 0.08 vs 3.75 ± 0.35 %ID/g, $p=0.0008$) (Fig. 5). As with the PET/CT results, there was no significant difference in ^{18}F -FFNP uptake in Y537S-ER tumors between the fulvestrant and control groups (2.68 ± 0.13 vs 3.24 ± 0.35 %ID/g, $p=0.8021$). As a positive control, ^{18}F -FFNP uptake in the uterus was lower in the fulvestrant group compared to control for both Y537S-ER ($p=0.0011$) and WT-ER ($p<0.0001$) tumor-bearing mice. Excised uteri weighed less in fulvestrant-treated mice compared to control (WT-ER tumor-bearing mice: 50 ± 8 vs 155 ± 25 mg, $p=0.0002$; Y537S-ER tumor-bearing mice: 60 ± 4 mg vs 193 ± 10 mg, $p=0.0001$), confirming appropriate dosing for ER antagonism.

PR immunohistochemistry results are in agreement with ^{18}F -FFNP tumor uptake. Decreased percentage of PR-positive cells and reduced staining intensity was observed in WT-ER tumors treated with fulvestrant, but not for Y537S-ER tumors (Supplemental Table 3; Supplemental Figure 3).

DISCUSSION

The study purpose was to determine how altered ER signaling caused by an activating *ESR1* mutation affects the prediction and early assessment of endocrine therapy response using molecular imaging. We demonstrated distinct growth phenotypes for tumor xenografts expressing Y537S-ER and WT-ER treated with estrogen or fulvestrant endocrine therapy. As expected, WT-ER tumors are strictly estrogen-dependent for growth with reduced tumor volumes in response to fulvestrant. In contrast, Y537S-ER tumors do not require estrogen for growth and are less sensitive to growth inhibition by fulvestrant compared to WT-ER. Baseline ^{18}F -FES uptake was not significantly different between Y537S-ER and WT-ER tumors. Likewise, early metabolic response was similar between both tumor types with decreased ^{18}F -FDG uptake in response to fulvestrant. However, ^{18}F -FFNP uptake decreased only in WT-ER tumors while ^{18}F -FFNP uptake was persistently elevated in Y537S-ER early after starting fulvestrant treatment. Differences in ^{18}F -FFNP uptake were observed prior to a change in tumor size. These results suggest that ^{18}F -FFNP PET imaging of PR expression dynamics could be an effective approach for early identification of reduced effectiveness of endocrine therapy resulting from activating *ESR1* mutations. The noninvasive approach and ability to assess response across multiple metastatic lesions are advantages of ^{18}F -FFNP PET imaging over repeated biopsies required for PR immunohistochemistry.

The clinical significance of *ESR1* mutations have only recently been recognized and testing is not yet routinely performed. Thus, tumor *ESR1* mutation status in previous clinical PET imaging studies of ER+ breast cancer are not known, with the exception of one report published earlier this year. Boers et al. investigated the relationship between inter-tumoral ^{18}F -FES heterogeneity and time to progression in metastatic ER+ breast cancer patients treated with

endocrine therapy combined with cyclin-dependent 4/6 kinase inhibition (14). *ESR1* mutations were present in circulating tumor DNA from 13 of 23 patients, but were not associated with ^{18}F -FES uptake (14).

We have previously shown that there was no alteration in measuring ER ligand binding with ^{18}F -FES in genetically engineered breast cancer xenografts expressing WT-ER or the constitutively active *ESR1* mutations, Y537S and Y537C (24). The triple-negative breast cancer model used in our prior study allowed testing ^{18}F -FES binding to mutant receptors in isolation from endogenous wild-type ER protein (24). ^{18}F -FES results from this study using CRISPR-edited T47D cells with heterozygous *ESR1* mutation expression are in agreement with our prior observations. Prospective testing for *ESR1* mutations in future studies of ^{18}F -FES PET imaging is important to validate these findings, particularly with recent FDA approval of ^{18}F -FES.

Similar early metabolic responses (reduced ^{18}F -FDG uptake) were observed in both WT-ER and Y537S-ER tumors in response to fulvestrant. This observation was unexpected based on our hypothesis that inhibition of glycolytic activity will be impaired in tumors expressing Y537S-ER treated with fulvestrant due to reduced endocrine sensitivity of the mutant receptor. Previous preclinical studies have demonstrated that fulvestrant treatment decreases ^{18}F -FDG uptake in ER+ breast cancer xenografts without known *ESR1* mutations. He et al. demonstrated reduced ^{18}F -FDG uptake in ER+ ZR-75-1 tumors after 21 days fulvestrant treatment when tumor volumes are decreased compared to vehicle control (28). We also demonstrated that ^{18}F -FDG uptake decreased after 7 and 14 days of fulvestrant treatment in endocrine-sensitive ER+PR+ STAT1-deficient mouse mammary tumors, SSM3, but remained unchanged in endocrine-resistant ER+PR+ SSM2 tumors (20). SSM2 tumors were completely resistant to fulvestrant with identical tumor growth rate compared to ethanol vehicle control, which differs from the growth

stabilization phenotype of Y537S-ER tumors observed in this study. Thus, the mechanism and magnitude of endocrine therapy resistance appears to affect the metabolic response pattern observed.

These results suggest that early assessment of PR expression dynamics could indicate insufficient ER signaling inhibition in tumors with activating *ESR1* mutations. Persistent ¹⁸F-FFNP uptake of Y537S-ER tumors after 7 days of fulvestrant was distinct from the reduced uptake seen with WT-ER tumors indicating inadequate therapy response despite maximal ER antagonist dosing. These results are in agreement with our previous preclinical studies demonstrating how changes in ¹⁸F-FFNP uptake reflect response to endocrine therapy in ER+PR+ STAT1-deficient tumors and provide predictive information beyond ¹⁸F-FES or ¹⁸F-FDG PET imaging (19,20). Collectively, ¹⁸F-FFNP appears to be a robust functional imaging biomarker of endocrine sensitivity and may be generalizable to endocrine therapy resistance acquired through different cellular mechanisms. Clinical trials confirming the predictive value of ¹⁸F-FFNP PET imaging in patients, such as the recently completed trial at Washington University (NCT02455453), are important for further validation.

The observed Y537S *ESR1* allele fraction in clinical samples from patients with metastatic breast cancer typically range between 23% and 62%, but can be as low as 4% (8). Thus, the 52% Y537S *ESR1* allele fraction present in the tumor model system used in our study appropriately represents the allele fractions found in metastases. However, the utility of serial ¹⁸F-FFNP imaging as a biomarker for response to fulvestrant for tumors with low Y537S *ESR1* mutation allele fractions would need to be directly tested.

This investigation focused on one *ESR1* mutation and one endocrine therapy agent. Other activating *ESR1* mutations may yield distinct results since mutation site-specific gene regulation

and anti-estrogen sensitivity has been recognized (7,10,29). Also, this work assessed ^{18}F -FES uptake prior to starting endocrine therapy, similar to the ongoing multicenter clinical trial (NCT02398773). It is possible that differences in residual ER binding capacity during fulvestrant treatment could be observed in tumors expressing activating *ESR1* mutations compared to wild-type. Imaging other pathways, such as glutamine metabolism, could also be informative for assessing therapy response since it has recently been demonstrated that Y53S-ER cells have similar glycolytic rates as WT-ER cells, but with enhanced mitochondrial activity and glutamine utilization (30).

CONCLUSION

These findings suggest that ^{18}F -FFNP PET imaging is capable of differentiating endocrine therapy effects in breast cancer with activating Y537S *ESR1* mutations. Our results also support *ESR1* mutation testing in clinical trials involving molecular imaging since distinct responses can occur with endocrine therapy depending on mutation status.

DISCLOSURE

UW-Madison Department of Radiology receives research support from GE Healthcare. No other potential conflicts of interest relevant to this article exist.

ACKNOWLEDGMENTS

We thank Dr. Steffi Oesterreich (University of Pittsburgh) for kindly providing cells. We thank the UW-Madison Cyclotron Laboratory for ^{18}F production, the Radiopharmaceutical Production Facility for ^{18}F -FFNP and ^{18}F -FES synthesis, and the Small Animal Imaging Facility

for technical support. We also thank the Translational Research Initiatives in Pathology laboratory, in part supported by the UW Department of Pathology and Laboratory Medicine and UWCCC grant (P30 CA014520), the Experimental Pathology Laboratory (P30 CA014520), and the UW-Madison Biophysics Instrumentation Facility, established with support from the UW-Madison and grants BIR-9512577 (NSF) and S10 RR13790 (NIH), for their services.

KEY POINTS

QUESTION: How do activating *ESR1* mutations affect the predictive values of ^{18}F -FES, ^{18}F -FDG, and ^{18}F -FFNP as endocrine therapy response biomarkers in ER+ breast cancer?

PERTINENT FINDINGS: ^{18}F -FFNP uptake decreased only in WT-ER tumors while ^{18}F -FFNP uptake was persistently elevated in Y537S-ER early after starting fulvestrant treatment.

IMPLICATION FOR PATIENT CARE: Early assessment of PR expression dynamics using ^{18}F -FFNP PET imaging could indicate insufficient ER signaling inhibition and inadequate therapy in tumors with activating *ESR1* mutations.

REFERENCES

1. Osborne CK, Schiff R. Mechanisms of endocrine resistance in breast cancer. *Annu Rev Med.* 2011;62:233-247.
2. Chandarlapaty S, Chen D, He W, et al. Prevalence of ESR1 mutations in cell-free DNA and outcomes in metastatic breast cancer: a secondary analysis of the BOLERO-2 clinical trial. *JAMA Oncol.* 2016;2:1310-1315.
3. Fribbens C, O'Leary B, Kilburn L, et al. Plasma ESR1 mutations and the treatment of estrogen receptor-positive advanced breast cancer. *J Clin Oncol.* 2016;34:2961-2968.
4. Katzenellenbogen JA, Mayne CG, Katzenellenbogen BS, Greene GL, Chandarlapaty S. Structural underpinnings of oestrogen receptor mutations in endocrine therapy resistance. *Nat Rev Cancer.* 2018;18:377-388.
5. Fanning SW, Mayne CG, Dharmarajan V, et al. Estrogen receptor alpha somatic mutations Y537S and D538G confer breast cancer endocrine resistance by stabilizing the activating function-2 binding conformation. *Elife.* 2016;5:e12792.
6. Nettles KW, Bruning JB, Gil G, et al. NFkappaB selectivity of estrogen receptor ligands revealed by comparative crystallographic analyses. *Nat Chem Biol.* 2008;4:241-247.
7. Zhao Y, Laws MJ, Guillen VS, et al. Structurally novel antiestrogens elicit differential responses from constitutively active mutant estrogen receptors in breast cancer cells and tumors. *Cancer Res.* 2017;77:5602-5613.
8. Toy W, Weir H, Razavi P, et al. Activating ESR1 mutations differentially affect the efficacy of ER antagonists. *Cancer Discov.* 2017;7:277-287.
9. Harrod A, Fulton J, Nguyen VTM, et al. Genomic modelling of the ESR1 Y537S mutation for evaluating function and new therapeutic approaches for metastatic breast cancer. *Oncogene.* 2017;36:2286-2296.
10. Bahreini A, Li Z, Wang P, et al. Mutation site and context dependent effects of ESR1 mutation in genome-edited breast cancer cell models. *Breast Cancer Res.* 2017;19:60.
11. Fanning SW, Jeselsohn R, Dharmarajan V, et al. The SERM/SERD basedoxifene disrupts ESR1 helix 12 to overcome acquired hormone resistance in breast cancer cells. *Elife.* 2018;7:e37161.

12. Mortimer JE, Dehdashti F, Siegel BA, Trinkaus K, Katzenellenbogen JA, Welch MJ. Metabolic flare: indicator of hormone responsiveness in advanced breast cancer. *J Clin Oncol*. 2001;19:2797-2803.
13. Linden HM, Stekhova SA, Link JM, et al. Quantitative fluoroestradiol positron emission tomography imaging predicts response to endocrine treatment in breast cancer. *J Clin Oncol*. 2006;24:2793-2799.
14. Boers J, Venema CM, de Vries EFJ, et al. Molecular imaging to identify patients with metastatic breast cancer who benefit from endocrine treatment combined with cyclin-dependent kinase inhibition. *Eur J Cancer*. 2020;126:11-20.
15. Kurland BF, Gadi VK, Specht JM, et al. Feasibility study of FDG PET as an indicator of early response to aromatase inhibitors and trastuzumab in a heterogeneous group of breast cancer patients. *EJNMMI Res*. 2012;2:34.
16. Mortazavi-Jehanno N, Giraudet AL, Champion L, et al. Assessment of response to endocrine therapy using FDG PET/CT in metastatic breast cancer: a pilot study. *Eur J Nucl Med Mol Imaging*. 2012;39:450-460.
17. Kurland BF, Peterson LM, Lee JH, et al. Estrogen receptor binding (18F-FES PET) and glycolytic activity (18F-FDG PET) predict progression-free survival on endocrine therapy in patients with ER+ breast cancer. *Clin Cancer Res*. 2017;23:407-415.
18. van Kruchten M, de Vries EG, Brown M, et al. PET imaging of oestrogen receptors in patients with breast cancer. *Lancet Oncol*. 2013;14:e465-475.
19. Chan SR, Fowler AM, Allen JA, et al. Longitudinal noninvasive imaging of progesterone receptor as a predictive biomarker of tumor responsiveness to estrogen deprivation therapy. *Clin Cancer Res*. 2015;21:1063-1070.
20. Fowler AM, Chan SR, Sharp TL, et al. Small-animal PET of steroid hormone receptors predicts tumor response to endocrine therapy using a preclinical model of breast cancer. *J Nucl Med*. 2012;53:1119-1126.
21. Salem K, Kumar M, Yan Y, et al. Sensitivity and isoform specificity of (18)F-fluorofuranylprogesterone for measuring progesterone receptor protein response to estradiol challenge in breast cancer. *J Nucl Med*. 2019;60:220-226.

22. Dehdashti F, Laforest R, Gao F, et al. Assessment of progesterone receptors in breast carcinoma by PET with 21-18F-fluoro-16alpha,17alpha-[(R)-(1'-alpha-furylmethylidene)dioxy]-19-norpregn-4-ene-3,20-dione. *J Nucl Med*. 2012;53:363-370.
23. Salem K, Kumar M, Klopping KC, Michel CJ, Yan Y, Fowler AM. Determination of binding affinity of molecular imaging agents for steroid hormone receptors in breast cancer. *Am J Nucl Med Mol Imaging*. 2018;8:119-126.
24. Kumar M, Salem K, Michel C, Jeffery JJ, Yan Y, Fowler AM. (18)F-Fluoroestradiol PET imaging of activating estrogen receptor-alpha mutations in breast cancer. *J Nucl Med*. 2019;60:1247-1252.
25. Sanchez-Criado JE, Trudgen K, Millan Y, et al. Estrogen receptor (ESR) 2 partially offsets the absence of ESR1 in gonadotropes of pituitary-specific *Esr1* knockout female mice. *Reproduction*. 2012;143:549-558.
26. Mortimer JE, Dehdashti F, Siegel BA, Katzenellenbogen JA, Fracasso P, Welch MJ. Positron emission tomography with 2-[18F]Fluoro-2-deoxy-D-glucose and 16alpha-[18F]fluoro-17beta-estradiol in breast cancer: correlation with estrogen receptor status and response to systemic therapy. *Clin Cancer Res*. 1996;2:933-939.
27. Ueda S, Tsuda H, Saeki T, et al. Early metabolic response to neoadjuvant letrozole, measured by FDG PET/CT, is correlated with a decrease in the Ki67 labeling index in patients with hormone receptor-positive primary breast cancer: a pilot study. *Breast Cancer*. 2011;18:299-308.
28. He S, Wang M, Yang Z, et al. Comparison of 18F-FES, 18F-FDG, and 18F-FMISO PET imaging probes for early prediction and monitoring of response to endocrine therapy in a mouse xenograft model of ER-positive breast cancer. *PLoS One*. 2016;11:e0159916.
29. Jeselsohn R, Bergholz JS, Pun M, et al. Allele-specific chromatin recruitment and therapeutic vulnerabilities of ESR1 activating mutations. *Cancer Cell*. 2018;33:173-186.
30. Zinger L, Merenbakh-Lamin K, Klein A, et al. Ligand-binding domain-activating mutations of ESR1 rewire cellular metabolism of breast cancer cells. *Clin Cancer Res*. 2019;25:2900-2914.

FIGURES

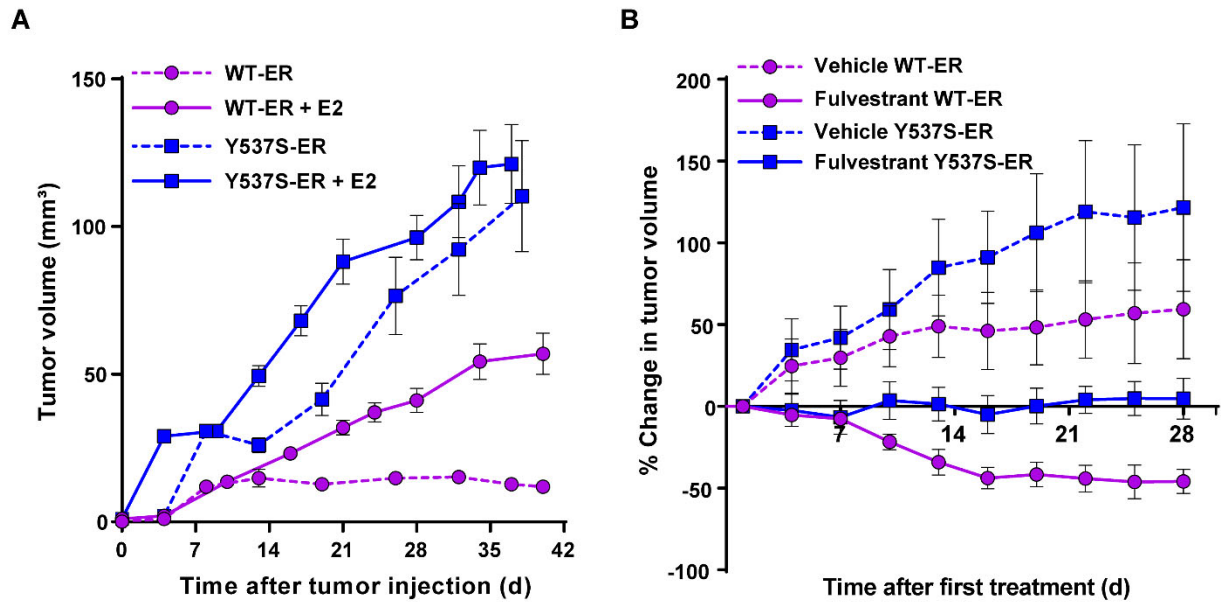


FIGURE 1. Estrogen-independent growth of Y537S-ER tumor xenografts and effect of fulvestrant treatment. (A) WT-ER and Y537S-ER tumor volumes for mice treated with or without 17 β -estradiol (E2); N=10 tumors/group/time point. (B) Percent change in tumor volumes following treatment with ethanol vehicle control or fulvestrant; N=12 tumors/group/time point.

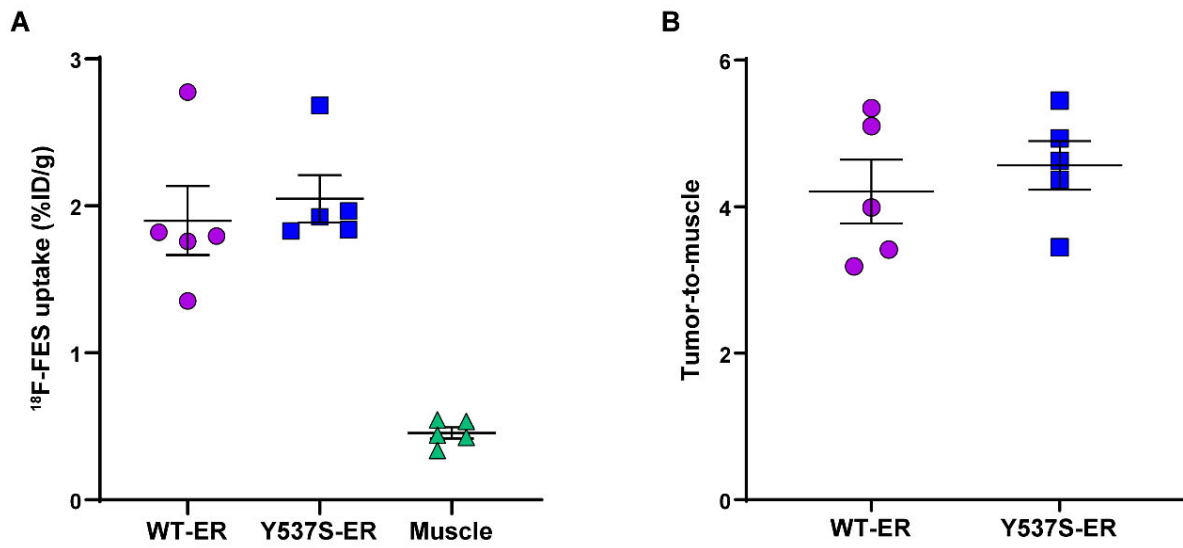


FIGURE 2. Baseline ^{18}F -FES uptake in WT-ER and Y537S-ER tumor xenografts. (A) Percent injected dose per gram (%ID/g) and (B) tumor-to-muscle uptake ratios. Estrogen in the drinking water was withdrawn 48 h prior to the ^{18}F -FES biodistribution assay.

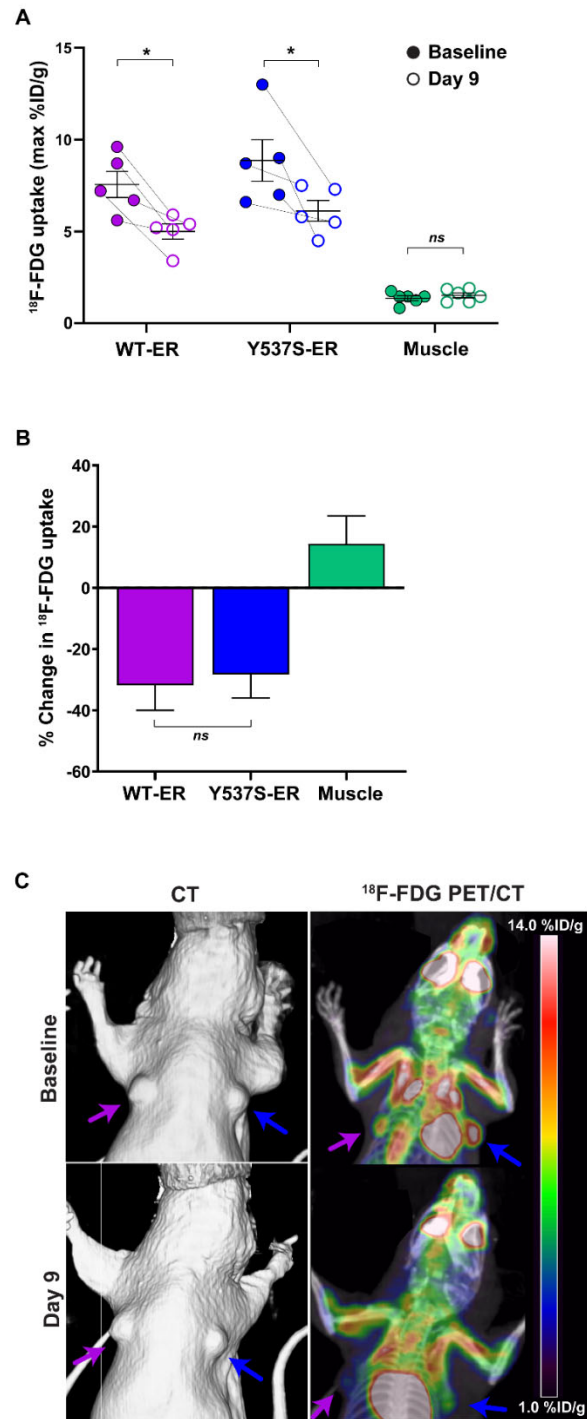


FIGURE 3. ^{18}F -FDG PET/CT of WT-ER and Y537S-ER tumor-bearing mice. (A) ^{18}F -FDG uptake at baseline and after 9 days of fulvestrant treatment (N=5 tumors/group). $P < 0.05^*$, ns=not significant. (B) Percent change in ^{18}F -FDG uptake. (C) Representative PET/CT images.

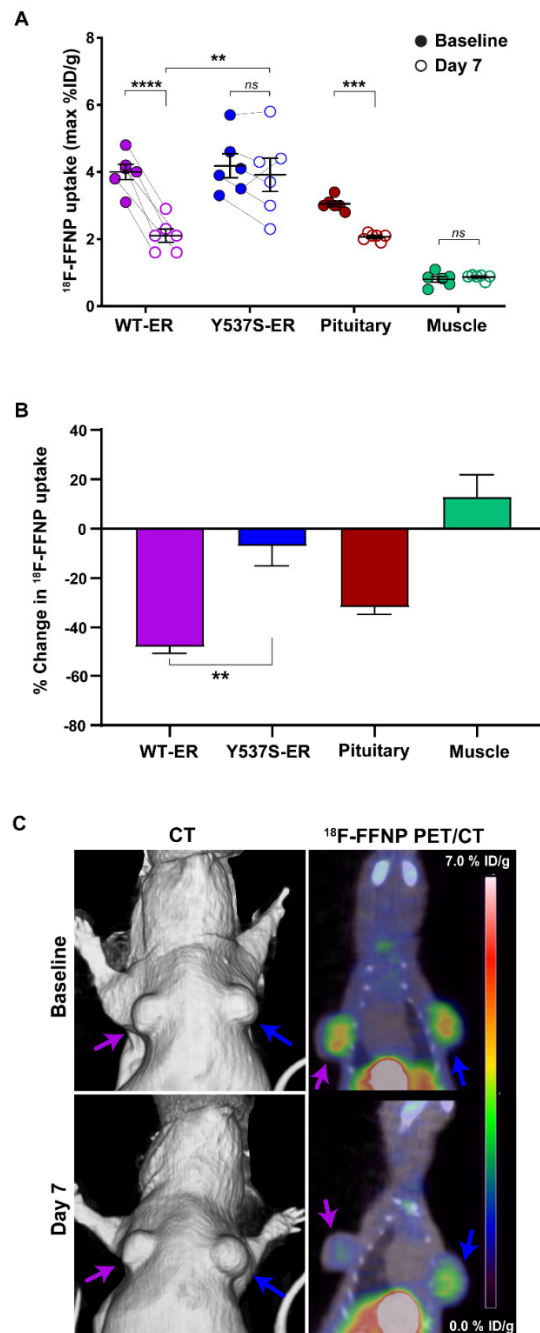


FIGURE 4. ^{18}F -FFNP PET/CT of WT-ER and Y537S-ER tumor-bearing mice. (A) ^{18}F -FFNP uptake at baseline and after 7 days of fulvestrant treatment (N=6 tumors/group). $P < 0.01^{**}$, $P < 0.001^{***}$, $P < 0.0001^{****}$, ns=not significant. (B) Percent change in ^{18}F -FFNP uptake. (C) Representative PET/CT images.

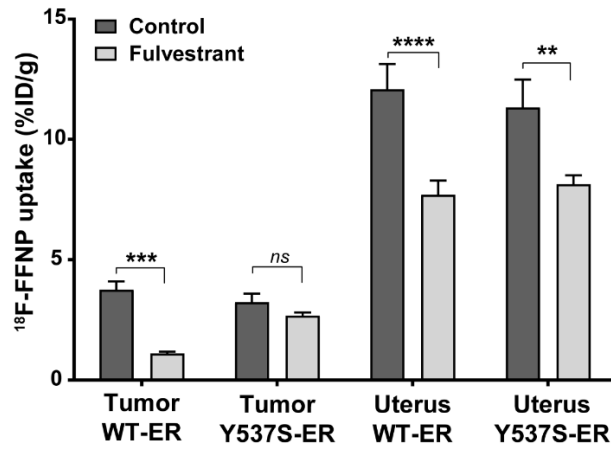


FIGURE 5. ^{18}F -FFNP tissue biodistribution assay. ^{18}F -FFNP uptake for mice bearing bilateral WT-ER tumors (N=8 tumors; 4 mice/treatment group) or bilateral Y537S-ER tumors (N=10 tumors; 5 mice per treatment group). $P < 0.01^{**}$, $P < 0.001^{***}$, $P < 0.0001^{****}$, ns=not significant.

SUPPLEMENTAL MATERIAL

Droplet Digital PCR Protocol

Reactions were prepared with 25 ng extracted DNA (DNeasy Blood & Tissue Kit, Qiagen) in ddPCR supermix for probes (Bio-Rad). *ESR1* primers were forward: 5'-GGCATGGAGCATCTGTACAG-3'; reverse: 5'-CAAGTGGCTTTGGTCCGTC-3'. WT-*ESR1* probe was 5'-HEX/CCCCTCTATGACCTGCTGCT-3'. Y537S-*ESR1* probe was 5'-56-FAM/CCCCTCTCTGACCTGCTGC/3IABkFQ-3' (Integrated DNA Technologies). Droplets were generated using Bio-Rad QX200 Droplet Generator using 20 μ L reaction mix with 70 μ L droplet generation oil. Droplets were then moved into a 96-well PCR plate and ran on C1000 Thermal Cycler (95 °C x 10 min, 40 cycles of 94 °C x 30 sec and 60 °C x 1 min, 98 °C x 10 min with a 105 °C heated lid). PCR products were then subjected to flow cytometry using QX200 Droplet Reader, measuring the equivalent of 10,000 genomic events. Mutation allele fractions were determined using QuantaSoft Analysis Pro v1.0.596 (Bio-Rad).

Supplemental Table 1: ^{18}F -FDG uptake values measured with PET/CT imaging

Treatment Group	Baseline (max %ID/g)	Treatment Day 7 (max %ID/g)	Baseline (T:M)	Treatment Day 7 (T:M)
WT-ER Tumor Control	8.30 ± 0.35	8.05 ± 1.04	6.37 ± 0.74	5.01 ± 0.77*
WT-ER Tumor Fulvestrant	7.56 ± 0.71	4.62 ± 0.79*	6.13 ± 1.37	3.66 ± 0.57*
Y537S-ER Tumor Control	10.24 ± 1.25	9.20 ± 1.00*	7.06 ± 0.86	5.39 ± 0.63
Y537S-ER Tumor Fulvestrant	8.86 ± 1.14	6.12 ± 0.57	6.84 ± 1.30	3.89 ± 0.37
Muscle Control	1.38 ± 0.10	1.65 ± 0.09	N/A	N/A
Muscle Fulvestrant	1.36 ± 0.09	1.46 ± 0.15	N/A	N/A

*Significant change in ^{18}F -FDG uptake when compared to baseline imaging (paired t-test; N=6 tumors per treatment group).

Supplemental Table 2: ¹⁸F-FFNP uptake values measured with PET/CT imaging

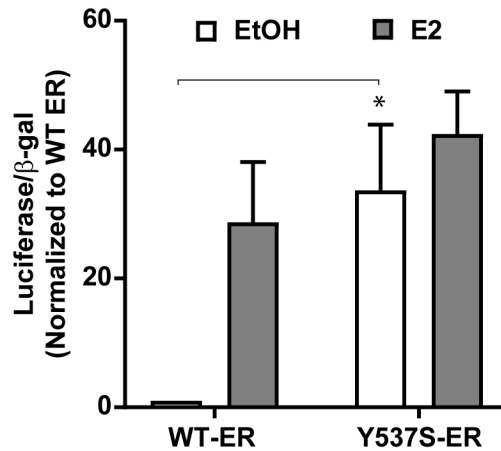
Treatment Group	Baseline (max %ID/g)	Treatment Day 7 (max %ID/g)	Baseline (T:M)	Treatment Day 7 (T:M)
WT-ER Tumor Control	3.97 ± 0.35	3.80 ± 0.31	4.95 ± 0.45	4.71 ± 0.36
WT-ER Tumor Fulvestrant	4.00 ± 0.23	2.10 ± 0.20*	5.26 ± 0.61	2.41 ± 0.18*
Y537S-ER Tumor Control	4.20 ± 0.19	3.75 ± 0.35	5.27 ± 0.54	4.61 ± 0.38
Y537S-ER Tumor Fulvestrant	4.18 ± 0.37	3.92 ± 0.50	5.41 ± 0.55	4.49 ± 0.50
Pituitary Gland Control	2.95 ± 0.07	3.17 ± 0.16	N/A	N/A
Pituitary Gland Fulvestrant	3.05 ± 0.08	2.07 ± 0.04*	N/A	N/A
Muscle Control	0.81 ± 0.04	0.84 ± 0.10	N/A	N/A
Muscle Fulvestrant	0.80 ± 0.08	0.87 ± 0.03	N/A	N/A

*Significant change in ¹⁸F-FFNP uptake when compared to baseline imaging (paired t-test; N=6 tumors per treatment group).

Supplemental Table 3: PR and ER immunohistochemistry of excised tumors

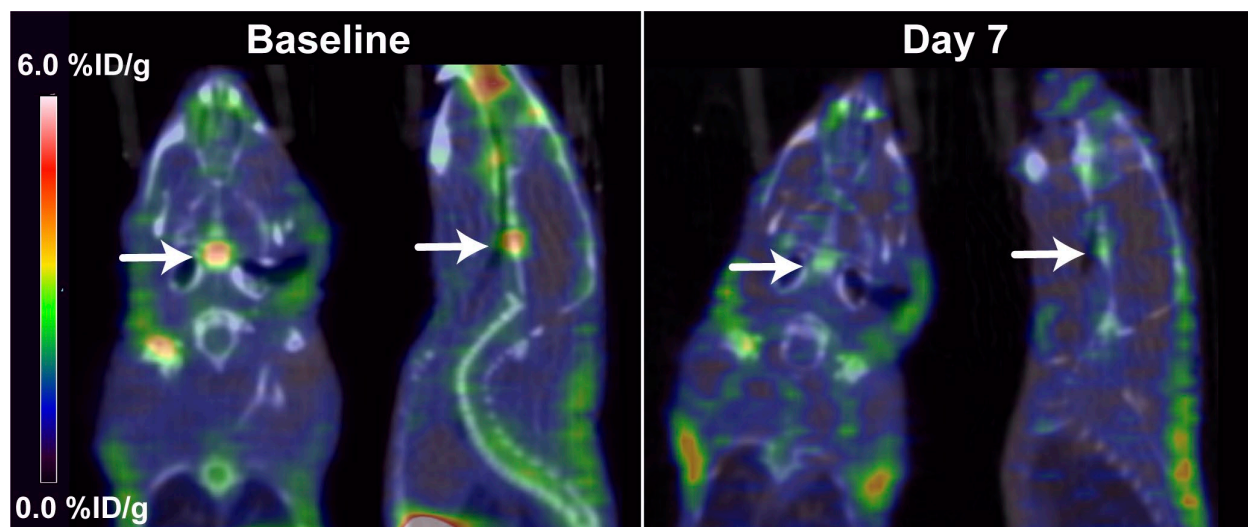
Treatment Group	PR+ (%)	PR Intensity	ER+ (%)	ER Intensity
WT-ER Tumor Control	94.00 ± 6.00	Strong (N=5/5)	41.0 ± 4.58	Moderate (N=2/5) Weak (N=3/5)
WT-ER Tumor Fulvestrant	56.25 ± 23.00	Moderate (N=4/4)	0	None (N=4/4)
Y537S-ER Tumor Control	80.00 ± 13.78	Strong (N=5/5)	46.4 ± 12.1	Moderate (N=1/5) Weak (N=4/5)
Y537S-ER Tumor Fulvestrant	80.00 ± 18.77	Strong (N=5/5)	0*	None* (N=5/5)

*Residual ER protein detectable by Western blot analysis (Supplemental Figure 3)

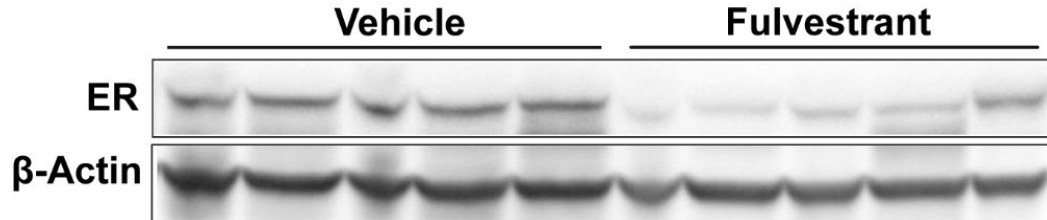


Supplemental Figure 1: Estrogen-dependent and estrogen-independent ER transcriptional activity of CRISPR-edited T47D breast cancer cells expressing WT-ER and Y537S-ER.

Cells were grown in steroid hormone-depleted media for 3 days and were seeded in a 6-well plate (500,000 cells/well). On day 5, cells were co-transfected with estrogen receptor response element (ERE)-luciferase (0.75 μ g) and cytomegalovirus- β -galactosidase (0.25 μ g) reporter plasmids using Lipofectamine 3000 (Life Technologies). The following day, cells were treated with ethanol (EtOH) vehicle or 10 nM 17 β -estradiol (E2) for 24 hours. Luciferase reporter gene activity (Promega) and β -galactosidase activity (Tropix) were measured according to the manufacturers' protocol. ERE-luciferase reporter gene activity was normalized to β -galactosidase activity to control for transfection efficiency. Data was normalized to WT-ER in the absence of E2 (N=3 independent experiments). * $P < 0.05$ compared to WT-ER.



Supplemental Figure 2: Representative horizontal/coronal and sagittal fused ^{18}F -FFNP PET/CT images demonstrating pituitary gland uptake (arrows) at baseline and 7 days after starting fulvestrant treatment.



Supplemental Figure 3: Western blot for ER and β -actin protein in the excised Y537S-ER tumors from the ^{18}F -FFNP biodistribution assay on day 7 post treatment with either ethanol vehicle control or fulvestrant. Tumor lysates were prepared from flash-frozen tumors excised on day 7 post treatment from the ^{18}F -FFNP biodistribution assay. Crushed flash-frozen tumors were lysed using radioimmunoprecipitation assay buffer (Sigma) with 2 mM sodium orthovanadate, protease (1:500) and phosphatase (1:100) inhibitor cocktails (Sigma). Protein concentration was determined with Bradford assay (Bio-Rad). Equal amounts of protein were run on 10% sodium-dodecyl sulfate-polyacrylamide gel electrophoresis (Bio-Rad) and transferred to a polyvinylidene difluoride membrane (Millipore). Saturating amounts of antibodies were used for ER (1:1,000 clone 6F11; Leica Biosystems), β -actin (1:20,000 clone AC-15; Sigma) as a loading control, and horseradish peroxidase-conjugated anti-mouse IgG (1:3,000; GE Healthcare).